

Available online at www.sciencedirect.com

jmr&t
Journal of Materials Research and Technology
journal homepage: www.elsevier.com/locate/jmrt



Effect of annealing treatment on mechanical properties of 3D-Printed composites



Sara Valvez ^a, Paulo N.B. Reis ^{b,*}, José A.M. Ferreira ^b

^a Department of Electromechanical Engineering, University of Beira Interior, 6201-001 Covilhã, Portugal

^b Department of Mechanical Engineering, CEMMPRE, University of Coimbra, 3030-194 Coimbra, Portugal

ARTICLE INFO

Article history:

Received 14 September 2022

Accepted 15 January 2023

Available online 21 January 2023

Keywords:

Additive manufacturing

Fused filament fabrication (FFF)

Thermal annealing

Mechanical properties

ABSTRACT

This study aims to analyse the annealing effect on the mechanical properties of PETG, carbon fibre reinforced PETG (PETG + CF) and Kevlar fibre reinforced PETG (PETG + KF). Regardless of the material, the final dimensions vary with temperature and exposure time, showing that the addition of fibres had no significant influence. On the other hand, the presence of fibres affects the radius of curvature, but this parameter shows to be very dependent on the type of fibre. In terms of hardness, higher temperatures and exposure times generally lead to higher values, achieving improvements of about 20% over untreated material. Regarding the bending properties, while they increase with exposure time and temperature for composites, in the case of neat PETG they increase with temperature and decrease with exposure time. Compared to untreated specimens, the maximum bending strength observed after the annealing treatment was 10.2%, 31.8% and 11.1% for PETG, PETG + CF and PETG + KF, respectively, while the maximum bending modulus was 17.6%, 61.1% and 62.6% higher, respectively. Benefits were also observed in terms of impact strength, stress relaxation and creep behaviour of all materials. For example, after annealing, lower stress relaxation and creep displacement values were observed.

© 2023 The Authors. Published by Elsevier B.V. This is an open access article under the CC BY-NC-ND license (<http://creativecommons.org/licenses/by-nc-nd/4.0/>).

1. Introduction

Additive manufacturing (AM) is a group of techniques that was developed to produce three dimensional models, layer-by-layer, combining several procedures, materials and equipment [1]. According to American Society for Testing and Materials (ASTM) [2], this technique can be divided into seven groups: 1) Vat photopolymerization, 2) Powder bed fusion, 3) Material extrusion, 4) Material jetting, 5) Sheet lamination, 6) Binder jetting, and 7) Directed energy deposition [3]. However, fused filament fabrication (FFF) is the most popular and is allocated to the material extrusion group [4]. In this case, a

continuous filament is extruded through a heated nozzle and precisely deposited layer by layer to form a printed part. However, in addition to the benefits associated with low-cost, high speed, relatively simple operating procedure and the ability to print parts involving multi-materials [5], some disadvantages are also recognized like appearance, poor surface quality [6], few diversities of thermoplastic materials suitable for the technique [4] and low mechanical properties [7–9].

Therefore, literature reports that optimizing the print parameters is crucial to obtain high mechanical performances. For example, according to Mohamed et al. [4], layer thickness, filament deposition width and orientation, as well as air gap (in the same layer or between layers) are the main processing

* Corresponding author.

E-mail address: paulo.reis@dem.uc.pt (P.N.B. Reis).

<https://doi.org/10.1016/j.jmrt.2023.01.097>

2238-7854/© 2023 The Authors. Published by Elsevier B.V. This is an open access article under the CC BY-NC-ND license (<http://creativecommons.org/licenses/by-nc-nd/4.0/>).

parameters that affect the mechanical properties of printed parts. However, due to the complex influence of printing parameters on the mechanical properties of the final part, it is important to evaluate their effect together in order to apply to real manufacturing conditions and respective applications [10]. According to Wang et al. [11], for example, smaller layer thicknesses promote higher tensile strength, because higher layer thicknesses create more interlayer gaps and, consequently, higher amount of air pores in the cross-section. Kovan et al. [12] reported that layer thickness and print orientation have a significant effect on the bonding strength of parts manufactured with FFF. In fact, gaps between rasters during 3D printing had negative effects on adhesion properties. Anitha et al. [13] found that layer thickness has the most important influence on the surface roughness and an inverse relationship can even be established between layer thickness and surface roughness. Nancharaiah et al. [14] observed that, by using a lower value of layer thickness and air gap, surface roughness could be improved due to the reduction of size and number of voids between layers. Reducing the size and number of gaps, the adhesion properties improve and, consequently, better mechanical properties are achieved. Gebisa et al. [15] reported that lower raster angles and higher raster width have the highest influence on the bending properties of the material. They found that low raster angle promotes higher bending properties because the filaments are deposited along the filaments' length and the bending load cuts most of the deposited rasters before the part breaks. Moreover, it was reported that thicker rasters can strengthen the part, because they can resist the applied load much better than thinner ones. Ahn et al. [16] found that using a negative air gap improves the mechanical properties of the materials. However, it was limited the lower value (than -0.0762 mm) because excess material can be accumulated on the nozzle and the part itself. Dawoud et al. [17] reported that a negative air gap of 0.05 mm can improve the tensile strength of the material. The reported benefits are attributed to the improved density of the printed parts, where the rasters can slightly overlap and generate a stronger interfacial bond between adjacent rasters. Moreover, positive air gaps lead to weak axial bonds due to the development of in-plane neighbouring cylindrical rasters that barely touch.

In addition to the printing settings, literature also emphasizes the benefits achieved with the post-process annealing on the final mechanical properties [18]. In fact, thermal annealing or heat treatment is the most popular post-processing method used to improve the strength and surface quality of FFF printed parts. Basically, this process consists of heating the polymer to a specific temperature, capable of promoting the molecular mobility of the polymer chains, keeping it at that temperature for a certain period of time and gradually cooling it to room temperature [19]. The temperature selected is generally higher than the glass transition temperature (T_g) in order to improve the polymer's crystallinity and, consequently, to obtain higher strength, thermal stability, impact strength, electrical properties and polymer toughness [20–22]. Hong et al. [23], for example, submitted PLA parts to an annealing treatment at 130 °C for 300 s and found a 58.3% increase in bending strength compared to the untreated PLA, while the compressive strength after treatment at 140 °C for

600 s increased by 39.8% . These improvements were justified by the increase in the interfacial bonding between layers due to the heat action. Kumar et al. [24] reported improvements of 7.8% , 8.5% , 5.5% and 9.4% in terms of hardness, tensile strength, impact strength and bending strength, respectively, for annealed PETG specimens when compared to PETG specimens without annealing treatment. The same properties were analysed for annealed PETG + CF and improvements of 14.8% , 22% , 12.1% and 10.5% , respectively, were found. These benefits were explained by the increasing of the interlayer diffusion bonding. According to El Magri et al. [25], annealing at a low heating/cooling rate improves significantly the crystallinity degree and consequently increase the tensile strength and Young's modulus of the parts. This improvement is related with a reduction in residual stresses and elimination of defects due to the post-processing treatment. Barkhad et al. [26] studied the effect of annealing on the mechanical and thermal insulation properties of compression-moulded PLA. When compared to untreated PLA, an increase in compressive strength and modulus of 84% and 73% was found, respectively. These benefits were attributed to the shaping of the crystals and spherulites during the annealing. Authors explained the improvement of the mechanical properties due to increased bonding of beads and crystallinity. D'Amico et al. [27] observed that sample's expansion in the direction perpendicular to the printed layer and deformations can occur after annealing above T_g due to residual stresses present in FFF parts. Wang et al. [28] reported that FFF parts relieve stress during printing through deformation. Moreover, Kantaros and Karalekas et al. [29] reported that finished parts still have residual stresses that may be relieved by annealing above T_g . Therefore, deformation is expected to be present in annealed samples because stress is relieved through deformation.

In this context, according to Arjun et al. [30], these two strategies independent of each other (process parameters and annealing treatment) are determinants for improving mechanical properties, but when combined, they allow to substantially maximize the mechanical performance of printed parts. However, Valvez et al. [31] observed that the annealing treatment affects the geometric and dimensional accuracy of the parts, which may even limit their applications for structural purposes. Both the benefits and limitations reported above were also corroborated by Patel et al. [32] and, in this context, they suggest further studies involving other materials and other mechanical properties in order to have a more complete understanding of the improvements obtained in parts obtained by FFF.

Therefore, this study aims to optimize the annealing parameters to neglect geometrical effects and maximize the mechanical properties of PETG, carbon fibre reinforced PETG (PETG + CF) and Kevlar fibre reinforced PETG (PETG + KF). For this purpose, temperatures of 90 °C, 110 °C and 130 °C as well as exposure times of 30 min, 240 min and 480 min will be considered. The geometrical and dimensional effects will be analysed in terms inverse of the sample's radius of curvature ($1/R$) and volumetric variation of the samples, while the mechanical properties analysed will be hardness, impact strength, flexural strength, and viscoelastic behaviour. Conclusions based on these considerations will be drawn, where

the effect of annealing treatment on viscoelastic behaviour will be focus of an analysis not yet available in the open literature.

2. Materials and experimental procedure

All samples were produced using a B2X300 FDM printer (supplied by BeeVeryCreative, Ilhavo, Portugal). The bulk material on a form of filament was extruded through a 0.6 mm hardened steel nozzle by a printing head and deposited on a heated platform in a user-defined pattern to achieve the desired flat shape.

The material used is Poly (ethylene terephthalate)-Glycol (PETG), which has chemical alkali resistance, transparency, gloss, low haze, good printability, among other benefits. These benefits are further enhanced by the addition of fibres where, for example, carbon fibres make the composite stronger and more resilient, as well as significantly reducing the risk of warping. As conveniently reported in Ref. [33], this makes it an excellent choice for the automotive sector and other industrial applications. On the other hand, when Kevlar fibres are added to a PETG matrix, the field of applications can be extended to sectors where high resistance to friction and impact are expected [33]. Therefore, based on these benefits, this study used commercially available PETG, PETG + CF and PETG + KF filaments. While PETG-based filaments containing aramid and carbon fibres were supplied by Nanovia (Louargat, France), neat PETG filament was supplied by FilTech (Baesweiler, Germany). All details of the materials can be found in the suppliers' datasheets.

For each material, different printing parameters were used to maximize the properties of each architecture, which are summarized in Table 1. For this purpose, a study based on the Taguchi method was previously developed to carry out the experimental procedure design, where the specimens were produced according to the L16 orthogonal array, and an analysis of variance (ANOVA) was performed, with 95% confidence interval, to assess the printing parameters effect on the bending properties. All these details can be found in Ref. [33], where the nozzle diameter and the bed temperature were always constant parameters with values of 0.6 mm and 80 °C, respectively.

Therefore, as shown in Fig. 1, all samples were printed with a raster angle (direction of deposition) of 0°, and Fig. 2 shows the dispersion state of CF and KF into polymer matrix. Although the fibre dispersion observed is from a PETG + CF composite, it is also representative of composites reinforced with Kevlar fibres. In this context, it is possible to conclude that there is a good dispersion of fibres in both composites (PETG + CF and PETG + KF) and an almost total absence of agglomerates.

Subsequently, immediately after printing, the samples were subjected to an annealing treatment in a Heraeus oven, model UT 6060 (supplied by Heraeus Noblelight GmbH, Hanau, Germany). The geometry of the samples used in this work is shown in Fig. 3, and Table 2 reports the temperature and exposure time used in this study for all materials. Both parameters were selected based on a study developed by Bhandari et al. [19], in which authors studied a similar polymer, and

ensuring that all temperatures are above the T_g of the materials. The specimens were laid upon a flat steel plate and placed in the oven which, after programmed temperature and time, were cooled still inside the oven to room temperature in order to maximize the crystallinity in the specimen [19].

Samples with dimensions of $85 \times 12.7 \times 4 \text{ mm}^3$ were used to evaluate the volume variation after annealing, and the average values were obtained by four measurements along its length and 10 measurements along its width and thickness. Finally, the curvature radius (R) of the specimens was obtained with a Mitutoyo PJ-P1010A profile projector, as shown in Fig. 4, and calculated by equation (1), that was based in trigonometrical formulations:

$$R = \frac{c^2 + 4d^2}{8d} \quad (1)$$

The inverse radius of curvature (1/R) was used to compare the annealing treatment effect on the final planeness of the samples. The hardness was obtained using an HMV-G Shimadzu tester according to the ASTM E 384-99 [34], where a load of 98.07 mN (HV 0.01) for 15 s was applied at room temperature. For each configuration, at least, 15 measurements were considered. Impact tests were carried out according to ASTM D256-04 [35] using samples with dimensions of $100 \times 10 \times 4 \text{ mm}^3$ and an Instron Ceast 9050 machine equipped with a pendulum of 5 J. For each condition, 10 specimens were tested at room temperature as shown in Fig. 5 (Fig. 5a). Finally, the bending tests were carried out according to ASTM D790-17 [36], using a Shimadzu universal testing machine, model Autograph AG-X, equipped with a 5 kN load cell, and a span of 64 mm). As shown in Fig. 5 (Fig. 5b), samples with $85 \times 12.7 \times 4 \text{ mm}^3$ were used and, for each condition, 5 specimens were tested at room temperature and at a displacement rate of 2 mm/min. The bending properties were obtained using the following equations [36,37]:

$$\sigma = \frac{3 P L}{2 b h^2} \quad (2)$$

$$E = \frac{\Delta P L^3}{48 \Delta u I} \quad (3)$$

where P is the load, L the span length, b the width, h the thickness of the specimen, I the moment of inertia of the cross section, ΔP the load range, Δu the bending displacement range in the mid span for an interval in the linear load-displacement region of the graph. The bending modulus (E) was obtained by linear regression of the load-displacement curves considering the interval in the linear segment with a correlation factor higher than 95% [37].

Regarding the viscoelastic behaviour, stress relaxation tests were carried out in the same machine (Shimadzu, model Autograph AG-X) and using the same device (see Fig. 5b), with similar samples to those used in the bending tests ($85 \times 12.7 \times 4 \text{ mm}^3$) and the same span (64 mm). The tests were carried out in accordance with ASTM E328-13 standard [38], where a fixed deflection/strain (correspondent to 50% of the maximum bending stress) is applied, and the bending stress recorded during the loading time (180 min). In this case, the deflection used correspond to 36.3 MPa, 40 MPa and 25 MPa for PETG, PETG + CF and PETG + KF, respectively. In terms of

Table 1 – Printing parameters used for each material.

Material	Nozzle diameter [mm]	Extruder temperature [°C]	Printing speed [mm/s]	Layer height [mm]	Infill [%]	Bed temperature [°C]
PETG	0.6	265	20	0.4	100	80
PETG CF	0.6	195	60	0.52	100	80
PETG KF	0.6	265	20	0.35	100	80

creep tests, they were carried out in the same machine and using the device shown in Fig. 5, with similar samples used in the stress relaxation ($85 \times 12.7 \times 4 \text{ mm}^3$) and with the same spam (64 mm). These tests were performed in accordance with ASTM D2990-09 standard [39], where a fixed stress/load is applied (36.3 MPa, 40 MPa and 25 MPa for PETG, PETG + CF and PETG + KF, respectively), and the displacement recorded during the loading time (180 min).

3. Results and discussion

The annealing treatment effect on the final dimensions of the samples was evaluated and Table 3 shows the results in terms of average volumetry and respective standard deviation (SD). It is possible to observe that both variables (temperature and exposure time) have a strong effect on the final dimensions of the samples. Positive variations mean that the specimens have increased in size, while negative variations indicate that the specimens have shrunk. For example, for neat PETG a difference of 10.5% is observed between the highest and lowest values obtained. However, this value is about 10.8% and 5.7% for PETG + CF and PETG + KF, respectively. In a more detailed analysis, compared to control samples, an exposure to 90 °C for 30 min increases the volumetry of all materials, but when the exposure time increases, whereas carbon fibre

reinforced composites show a tendency to decrease, the other materials show a slight upward trend. Compared to the temperature of 110 °C, regardless of the material, an exposure time of 30 min promotes an increase in volume, but for higher values there is a decrease, reaching, particularly in composites, dimensions even smaller than those observed for control samples. Finally, for the temperature of 130 °C, an exposure time of 30 min causes an increase in volume, except for carbon fibre reinforced composites that shrink. However, when the exposure time increases, the dimensions of the specimens decrease, even to values lower than those of the untreated specimens, except for Kevlar composites that show a slight tendency to increase.

Therefore, the addition of fibres to the matrix has no substantial influence on the dimensional variation, nor does it establish a clear trend (increase or decrease). In fact, the annealing treatment promotes a competition of phenomena, which are even more expressive when fibres are added to the matrix. For example, shrinkage after annealing is expected due to densification of the crystal structure and increased bonding [40]. On the other hand, thermal annealing relieves residual stresses and, consequently, promotes an expansion in the layering. These residual stresses are unavoidable because they result from the printing process. For example, whenever there is a layer deposition, there is a cooling of the extrusion temperature to approximately the chamber

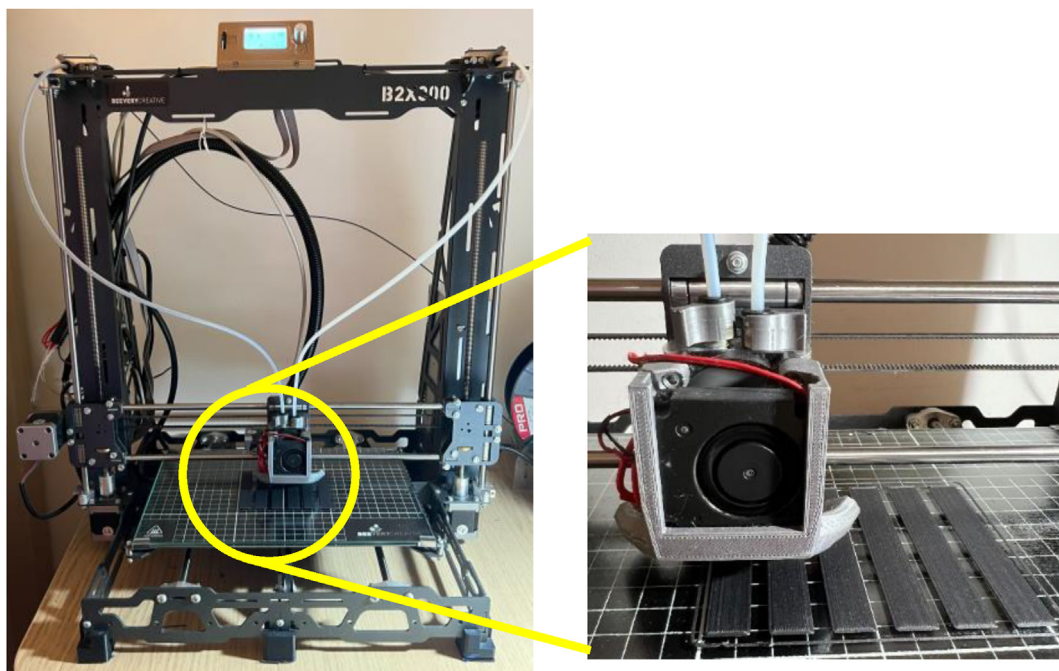


Fig. 1 – Details of the 3D printer producing a specimen in an environmentally controlled room.

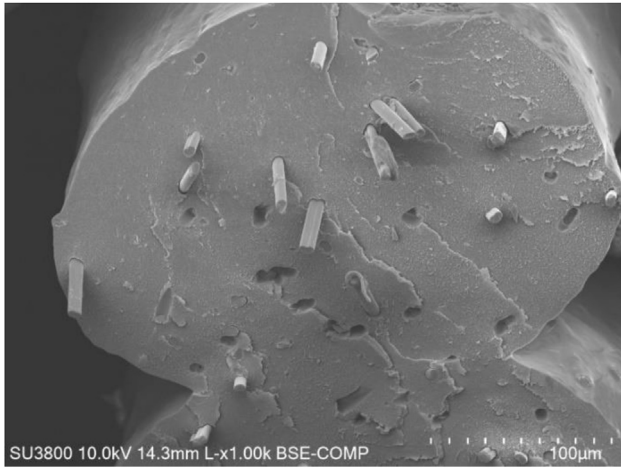


Fig. 2 – Dispersion state of CF and KF into polymer matrix.

temperature, but the next deposition instantly raises the temperature of the previous layers to close to the extrusion temperature, causing a large and sudden expansion of the previous layers, introducing, in this case, thermal stresses [41]. Furthermore, dimensions can be affected in any of the three axes (x, y and z) due to shrinkage or expansion that results from how the samples cool and how the stresses and air bubbles become locked between the layers [42]. In this case the randomness of the results is even higher and, for example, an analysis in terms of individual dimensions (length, width, and thickness) reveals that PETG and PETG + CF shrink along the length, while expansion and contraction occur for PETG + KF. In terms of thickness, it was found that all materials expanded, with the highest values observed for PETG + CF, while the lowest ones were very close for neat PETG and PETG + CF. Valvez et al. [33], for example, analysed the thermal conductivity of these materials and found that the highest value occurs for PETG + CF, because carbon fibres are excellent thermal conductors [43,44]. Therefore, thermal annealing is expected to relieve more residual stresses in this material than in the others and, consequently, promote higher expansion [41]. Finally, in terms of width, it was observed that neat PETG expands for all analysed conditions (temperature and time), while PETG composites showed a randomness between expansion and shrinkage. For example,

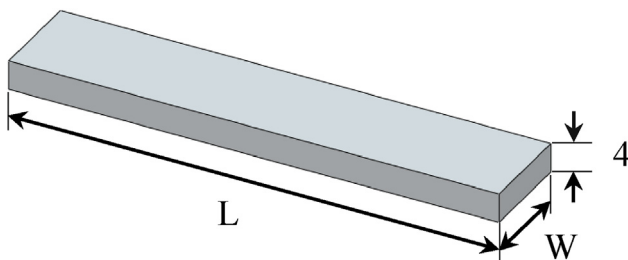


Fig. 3 – Geometry of the specimens (L = 85 mm and W = 12.7 mm for static and viscoelastic bending tests, and L = 100 mm and W = 10 mm for impact tests).

Table 2 – Annealing parameters for all materials.

Samples group	Temperature [°C]	Time [min]
1	90	30
2	90	240
3	90	480
4	110	30
5	110	240
6	110	480
7	130	30
8	130	240
9	130	480

Fig. 6 shows this evidence, where in Fig. 6a) the first image on the left illustrates a sample subjected to 90 °C for 30 min (sample group 1 of Table 2) and the last image on the right illustrates a sample subjected to 130 °C for 480 min (sample from group 9, from Table 2). Regardless of whether the image illustrates the dimensional variations for PETG composites with carbon fibres, it is representative of all materials. Therefore, this detailed analysis by axis (Fig. 6a and b) shows that, due to the randomness of the values obtained, there is no preponderant dimension over the others in terms of expansion/shrinkage, nor is it possible to establish a clear trend regarding the effects of the annealing treatment.

Regarding the radius of curvature (R), Table 4 presents this parameter in terms of inverse radius of curvature (1/R) to compare the effect of the annealing treatment on the geometry of the samples.

Different from volume variation, the presence of fibres affects the radius of curvature, but this parameter shows to be very dependent on the type of fibre. For example, while composites involving Kevlar fibres bend at temperatures above 110 °C (and for any exposure time), those reinforced with carbon fibres bend only at temperatures of 130 °C and exposure times higher than 240 min. On the other hand, the neat polymer (PETG) bend for all temperatures and exposure times, except for the temperature of 90 °C and exposure times of 30 min and 240 min. According to the literature, this can be explained by the internal stresses that occur during the cooling phase and act mainly in the upper layers of the samples [45]. The deposited layers can present three phases during their thermal history: solid phase, molten state, and cooling/solidification. In this context, each layer experiences a different thermal history and, due to uneven heating of the samples, interlayer stresses easily arise that promote sample's deformation [46]. On the other hand, the increase in crystallization due to the annealing process leads to less curvature of the sample [45]. Therefore, the competition of these two phenomena explains the curvature of the specimens, but it is not surprising that higher temperatures and exposure times lead to smaller radius of curvature due to a higher crystallization of the specimen.

In terms of hardness, Table 5 shows the average values obtained for the different materials and test conditions analysed.

For all materials, it is possible to observe that higher temperatures and exposure times generally lead to higher hardness values. This is due to lower internal stresses and more uniform connections between layers [42]. On the other hand,

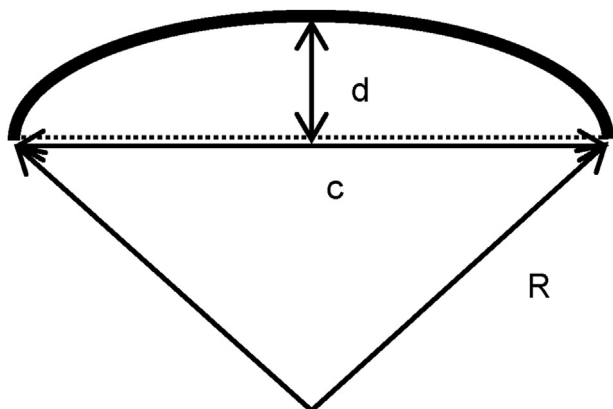


Fig. 4 – Scheme used to determine the (R).

annealing treatments reduce the surface roughness, which can lead to higher hardness values. Nevertheless, regardless of whether annealing reduces surface roughness, the indenter may encounter a peak or a valley which, due to non-uniform contact, justifies the observed dispersion [42].

Regarding the bending properties, the annealing effect was studied using three-point bending tests, and Figs. 7–9 show typical bending stress-strain curves for all materials. They are representative of all others obtained for each configuration. It is possible to observe a linear increase of the bending stress with the strain (linear elastic region), followed by a non-linear behaviour in which the maximum bending stress is reached. Kevlar composites are an exception to this behaviour, where a brittle behaviour is observed for the highest temperature (130 °C). It is also possible to notice that, in general, the annealing treatment promotes longer linear regimes as well as higher bending stress and modulus. On the other hand, the strain at maximum bending stress decreases. Another evidence is that, in this treatment, both temperature and exposure time influence the mechanical properties, but in a different way between the neat polymer and the fibre reinforced one.

Failure modes are shown in Fig. 10 for neat PETG and PETG + KF composites (which is also representative of PETG + CF) and for samples subjected to a temperature of 110 °C and an exposure time of 30 min. However, they are representative of all conditions analysed in this study.

In terms of neat PETG (Fig. 10a), it is possible to observe that the main damage mode occurs by plastic deformation, which increases from the neutral axis to the external fibre where the tensile stress is maximum (see top and lateral views in Fig. 10a). In this case, there is no sample breakage or visible cracks, but some microcracks are also expected due to the interlayer debonding that can be favoured by the existing voids. In terms of composites (Fig. 10b), it is notable the existence of cracks that start at maximum bending stress point, which result from the mixed mode of failure and consequent rupture of the printed layers. The micrograph in Fig. 10b shows, for example, fibre fracture and the pulling of some fibres from the matrix occurring simultaneously. This is explained by the fact that, in the first case, both the adhesion and the length of the fibre wetted by the matrix present high enough values to support the shear stresses that occur along the fibre/matrix interface. On the other hand, the opposite situation leads to fibre pull-out because the shear stresses at the interface are not sufficient to prevent slippage. This micrograph, when compared to Fig. 2, also shows that the annealing treatment does not affect the dispersion of the fibres in the matrix. In this case, the absence of fibre agglomeration does not compromise the benefits reported in the literature [47–49]. The agglomeration results in defects, which act as local stress concentrations and the consequent decrease in the mechanical performance of the composite. In addition, the fibres are not completely wetted by the resin and limit their main function within the polymer matrix related to stress transfer [47,50,51].

A detailed analysis based on the previous curves is summarized in Table 6 and Table 7 for the maximum bending stress and bending modulus, respectively. These tables present the mean values and respective standard deviations for all materials and conditions analysed. Therefore, it is possible to observe that, for both properties, there are two different behaviours. In terms of neat PETG, for example, bending

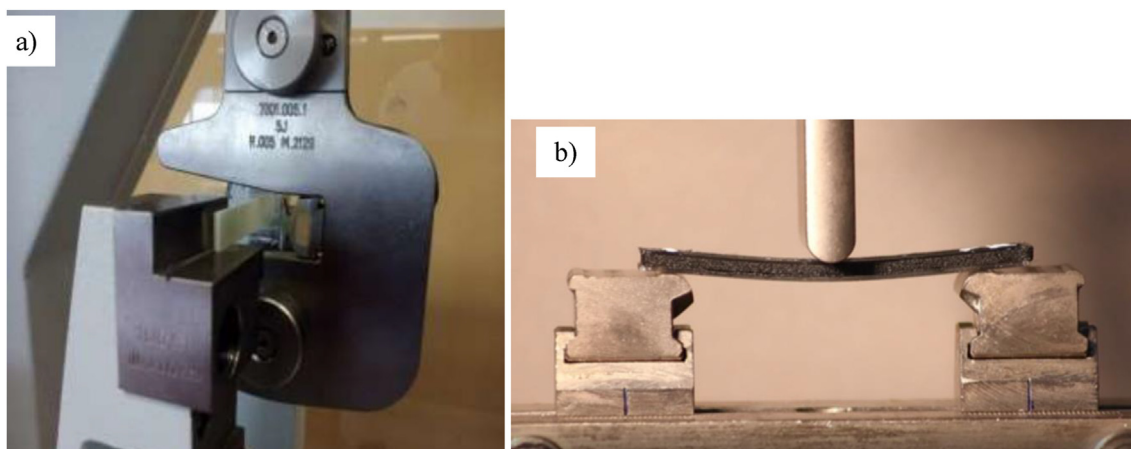


Fig. 5 – Device used in: a) Impact tests; b) Bending tests (for static and viscoelastic tests).

Table 3 – Volume variation after the annealing heat treatment.

Samples Group	PETG		PETG + CF		PETG + KF	
	[mm ³]	Variation [%]	[mm ³]	Variation [%]	[mm ³]	Variation [%]
Control	4171 ± 38.7	–	4575.0 ± 21.9	–	4513.3 ± 47.1	–
1	4271.4 ± 50.3	+2.4	4732.8 ± 38.6	+3.4	4689.5 ± 159.0	+3.9
2	4260.9 ± 25.5	+2.2	4636.7 ± 37.9	+1.3	4565.3 ± 52.4	+1.2
3	4295.4 ± 35.0	+3.0	4594.6 ± 103.3	+0.4	4715.8 ± 47.6	+4.5
4	4313.8 ± 46.4	+3.4	4761.9 ± 49.4	+4.1	4614.6 ± 71.8	+2.2
5	4170.9 ± 35.6	-2.4 × 10 ⁻⁵	4476.8 ± 5.2	-2.1	4460.2 ± 55.8	-1.2
6	4175.2 ± 93.2	+0.1	4479.6 ± 34.4	-2.1	4507.8 ± 60.8	-0.1
7	4416.9 ± 34.5	+5.9	4445.1 ± 22.3	-2.8	4604.1 ± 118.1	+2.0
8	3998.2 ± 45.1	-4.1	4427.9 ± 74.4	-3.2	4711.7 ± 56.7	+4.4
9	4048.1 ± 62.0	-2.9	4296.1 ± 29.0	-6.1	4642.4 ± 66.4	+2.9

strength and stiffness increase with temperature, while exposure time leads to an opposite trend, regardless of the annealing temperature studied. Regarding the composites, both properties generally increase with exposure time and temperature. However, a more detailed analysis reveals that the maximum bending strength for neat PETG is obtained for 130 °C and an exposure time of 30 min, leading to an increase of 10.2% over the control specimens, while for composites it occurs for the highest temperature and exposure time (130 °C and 480 min). In this case, the improvements are around 31.8% for composites with carbon fibres and 11.1% for composites with Kevlar fibres.

The bending modulus for neat PETG presents the highest value for temperatures of 90 °C and 130 °C (in both cases with an exposure time of 30 min) and promoting improvements of around 17.6% in relation to the control samples. In terms of composites reinforced with carbon fibres, the highest value occurs for the highest temperature and exposure time (130 °C and 480 min) with an improvement of 61.1% compared to the control samples. On the other hand, for composites reinforced with Kevlar fibres, the highest bending modulus occurred for 90 °C and an exposure time of 240 min, which is 62.6% higher than the value observed for the control specimens.

Therefore, the benefits observed for the polymer can be explained by the crystallinity of the material and the cross-linking of the molecular chains. In this case, higher

temperatures accelerate the interlayer diffusion of polymer molecules and promote stronger bonds (consequently better mechanical properties) [52–56]. Higher temperatures also provide more energy to increase the crystallinity degree [42,57–59], however, in this case, longer exposure times are not recommended due to the thermal degradation of the polymer [60,61]. In terms of composite materials, other variables must also be considered to explain the mechanical properties obtained, such as the voids between adjacent filaments and the degree of diffusion at the interfaces (resulting from a complex print history) [57]. In the case of voids, there is consensus that both filaments and printed parts have more voids than bulk materials. For example, while in filaments they result from bubbles formed by entrained air during the addition of fillers to the polymer, in printed material they result from constraints (clogging, abnormal feed flow) in the extruder nozzle during printing [62]. In this context, higher temperatures and exposure time are favourable, because they reduce voids (the material fills more voids) and, consequently, increases the interlayer bonding (higher interlayer strength), [19,63,64]. In this process, the different viscosity that occurs during the annealing treatment is decisive in filling the voids, but also because it promotes a minimization of the internal molecular stresses with the consequent internal reorganization (relaxation of the polymeric structure and reorientation of the polymeric chain structure towards the fillings) [25].

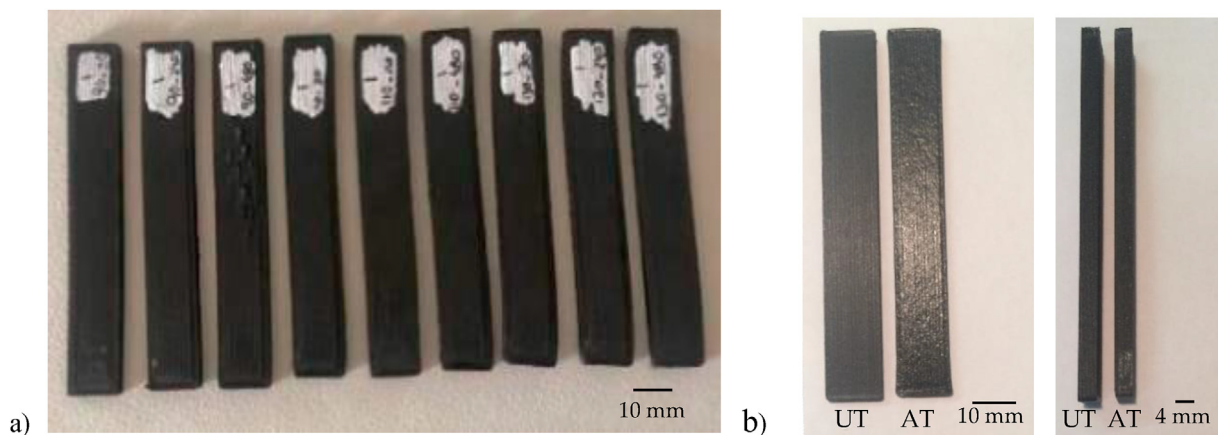


Fig. 6 – Dimensional changes: a) For all annealing conditions; b) Comparison between a sample subjected to annealing (130 °C for 240 min) (AT) with an untreated one (UT).

Table 4 – Inverse radius of curvature (1/R) after the annealing treatment. Dimensions in mm.

Samples Group	PETG		PETG + CF		PETG + KF	
	[mm]	Variation [%]	[mm]	Variation [%]	[mm]	Variation [%]
Control	0	–	0	–	0	–
1	0	–	0	–	0	–
2	0	–	0	–	0	–
3	$4.3 \times 10^{-4} \pm 8.7 \times 10^{-6}$	–	0	–	0	–
4	$7.9 \times 10^{-4} \pm 8.2 \times 10^{-6}$	–	0	–	$1.1 \times 10^{-3} \pm 1.5 \times 10^{-5}$	–
5	$1.3 \times 10^{-4} \pm 1.4 \times 10^{-6}$	–	0	–	$1.4 \times 10^{-3} \pm 2.9 \times 10^{-5}$	–
6	$1.5 \times 10^{-3} \pm 1.2 \times 10^{-5}$	–	0	–	$1.7 \times 10^{-3} \pm 3.7 \times 10^{-5}$	–
7	$1.8 \times 10^{-3} \pm 1.9 \times 10^{-5}$	–	0	–	$1.8 \times 10^{-3} \pm 1.5 \times 10^{-5}$	–
8	$2.1 \times 10^{-3} \pm 1.8 \times 10^{-5}$	–	$5.1 \times 10^{-4} \pm 1.7 \times 10^{-5}$	–	$2.1 \times 10^{-3} \pm 2.7 \times 10^{-5}$	–
9	$3.5 \times 10^{-3} \pm 4.8 \times 10^{-5}$	–	$2.3 \times 10^{-4} \pm 2.1 \times 10^{-5}$	–	$2.7 \times 10^{-3} \pm 1.5 \times 10^{-5}$	–

Finally, for any composite and regardless of the manufacturing process, the adhesion properties between filler-matrix are also very important to improve the mechanical properties of a composite material. In this context, literature acknowledges the good fibre/matrix adhesion for glass and carbon fibres, while Kevlar fibres are recognized for establishing a weak fibre/matrix adhesion [65], which justifies the results obtained. In fact, composites reinforced with Kevlar fibres showed the worst results due to poor fibre/matrix adhesion. Therefore, if there is no degradation of the material, the increase in temperature and exposure time promotes an improvement of bending properties by increasing the interfacial bond between the rasters [23].

Charpy impact tests were also performed to study the annealing effect on the impact strength, and the results obtained for the different conditions analysed are shown in Fig. 11. Impact strength is defined as the resilience value at break point [66], and it should be noted that the conditions used for the annealing treatment are 90 °C and 30 min for PETG and 90 °C and 240 min for PETG + CF and PETG + KF, respectively. These treatments were selected to combine the maximization of the properties reported in Tables 5–7 with the minimization of the geometric effects reported in Tables 3–4. It is also worth mentioning that the printing parameters were different for the different materials, which aimed to maximize the bending properties of each one of them. For these conditions, it is possible to observe from Fig. 11a) that the highest impact strength is obtained for neat PETG, but when carbon and Kevlar fibres are added, this value decreases around 82.6% and 89.5%, respectively. In terms of energy absorbed (Fig. 11b), the neat polymer has the highest value

(78.9%), but when fibres are added this value decreases in proportions very similar to those reported previously.

On the other hand, it is possible to observe that the annealing treatment improves the impact strength for all analysed materials. Compared to untreated specimens, the highest improvement was observed for PETG + KF with 16%, followed by PETG (8.1%) and PETG + CF (3.5%). In addition to the intrinsic properties of the materials that explain these results, literature also reports that the impact properties are mainly influenced by porosity, molecular bonding, and inter-layer adhesion, which depend on printing parameters [67]. In fact, the presence of voids decreases the amount of material capable of absorbing impact energy [67,68]. Therefore, the annealing treatment proves to be beneficial, and the observed improvements can be explained by the increase in the inter-layer bonding due to the filling of voids by some material [19].

Finally, the annealing effect on stress relaxation and creep behaviour is shown in Fig. 12. The annealing treatments were similar to those used in the impact study and the tests carried out for stress levels corresponding to 50% of the maximum bending stress.

In terms of stress relaxation, Fig. 12a) plots the average bending stress versus time, where σ is the bending stress at any given moment of the test and σ_0 is the initial bending stress. As expected, a decrease in stress is observed that does not reach a constant value because it is a short-term test. However, these tests represent an easy, fast, and reliable method to predict long-term behaviour [69].

For untreated materials, it is possible to observe that the material with the lowest sensitivity to stress relaxation is neat PETG, while the most sensitive is PETG + CF. In the first case,

Table 5 – Annealing treatment effect on the hardness.

Samples Group	PETG		PETG + CF		PETG + KF	
	[MPa]	Variation [%]	[MPa]	Variation [%]	[MPa]	Variation [%]
Control	9.8 ± 0.3	–	11.7 ± 0.8	–	11.7 ± 0.9	–
1	11.2 ± 0.4	13.4	12.4 ± 0.7	5.6	11.9 ± 1.2	1.3
2	10.4 ± 0.8	5.3	12.8 ± 1.0	9.2	12.0 ± 0.9	2.3
3	10.7 ± 0.3	8.4	13.4 ± 0.5	14.3	12.2 ± 1.0	3.8
4	11.7 ± 0.5	19.2	12.5 ± 0.9	7.1	12.5 ± 0.4	6.4
5	10.3 ± 0.3	4.8	12.9 ± 0.5	10.1	12.9 ± 0.8	10.5
6	10.5 ± 0.5	7.2	14.0 ± 1.2	19.6	13.1 ± 0.9	11.7
7	10.8 ± 0.5	9.9	12.3 ± 0.9	4.9	13.4 ± 1.2	14.8
8	10.8 ± 0.2	9.3	13.0 ± 0.9	11.2	14.1 ± 0.6	20.2
9	11.0 ± 0.3	11.9	14.8 ± 0.9	26.1	14.2 ± 0.7	21.6

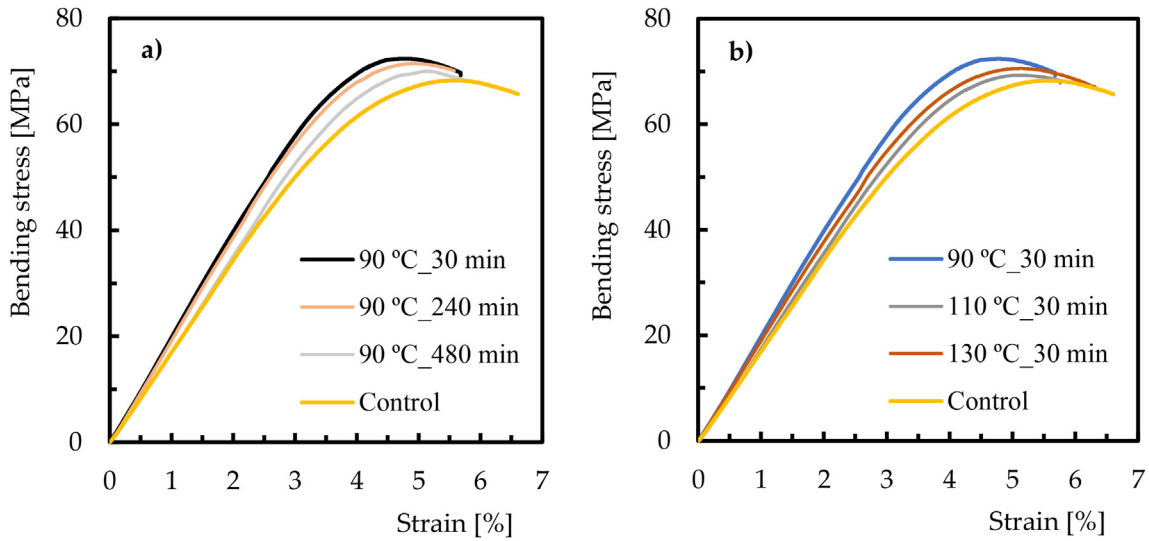


Fig. 7 – Bending stress-strain curves for PETG showing the effect of: a) Exposure time; b) Temperature.

the stress decreases by 10.5% in relation to its initial value, while for composites reinforced with carbon fibres this value is around 19.4%. PETG + KF composites lie between the two with a decrease of 13.9%. In terms of neat polymer, this decreasing is explained by molecular rearrangements that require little formation or rupture of primary bonds, while from a chemical point of view by the chain scission, crosslink scission or crosslink formation [70–72]. In addition, for printed materials, any decohesion that may occur between the printed interface layers or voids between adjacent printed layers contribute to a further decrease [73]. On the other hand, when polymers are reinforced with fibres, they hinder the molecular flow in the matrix and, consequently, delay the relaxation process [74]. In this case, the interface properties are decisive because relaxation is due to the breaking of bonds and their propagation. One more time, the voids between adjacent printed layers contribute to a further decrease in

stress [73]. However, contrary to what would be expected, the fibres seem to induce higher sensitivity. For example, in terms of PETG + KF, this material is subject to a bending strain corresponding to an initial bending stress of 23.8 MPa (29% lower than that applied to neat PETG) and, even then, it relaxed more than neat polymer (10.5% and 13.9%, respectively). This is clear evidence that, for the same bending strain, the PETG + KF composite would relax more than neat PETG, revealing a weak fibre/matrix interface, as well as the existence of voids already reported. In addition, Kevlar fibres have a polymeric nature, making them more sensitive to stress relaxation and creep behaviour than carbon and glass fibres [75]. In terms of PETG + CF composite, which presents the highest stress relaxation, it should be noted that the test was performed with a bending strain corresponding to a bending stress of 39.5 MPa (17.7% higher than that of neat PETG). Even so, the bending stress after 180 min was higher than the initial

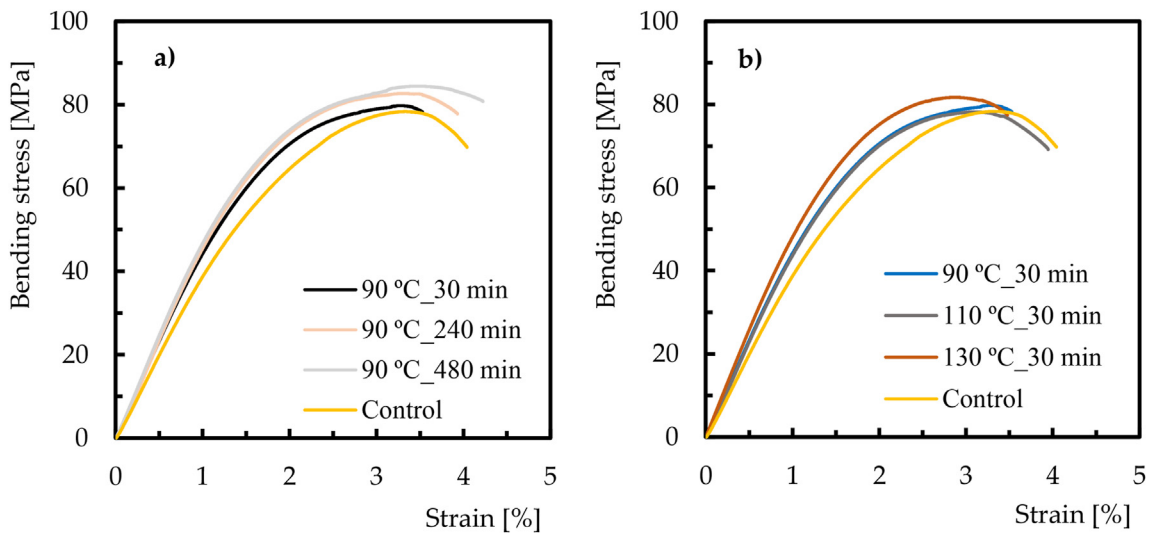


Fig. 8 – Bending stress-strain curves for PETG + CF showing the effect of: a) Exposure time; b) Temperature.

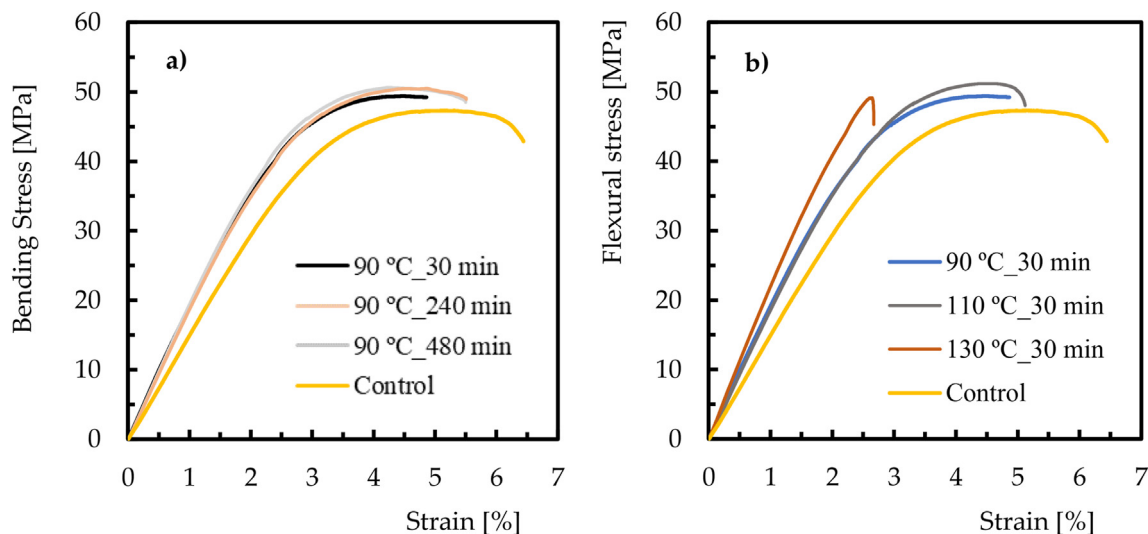


Fig. 9 – Bending stress-strain curves for PETG + KF showing the effect of: a) Exposure time; b) Temperature.

value used for neat PETG. In fact, increased bending strain promotes higher stress relaxation due to changes in mechanisms. For smaller bending strains, the stress relaxation is mainly induced by the molecular rearrangements and/or chain scission, while for higher bending strains it is due to damage and its propagation [73]. In the latter case (higher bending strains), the phenomenon becomes more expressive because voids already exist.

The same analysis reported above can be extended to the annealed materials, but in this case the decrease in bending

stress after 180 min of testing was only 3% for neat PETG, 6.8% for PETG + CF composite and 6.3% for the PETG + KF composite. In relation to the values obtained for the untreated specimens, these values are 71.8%, 64.7% and 54.5% lower, respectively. As mentioned before, this improvement is due to lower voids content and higher strength between layers obtained with the annealing treatment [19].

Concerning the annealing effect on the creep behaviour, Fig. 12b) shows the displacement-time curves for each material. The annealing treatments were similar to those reported

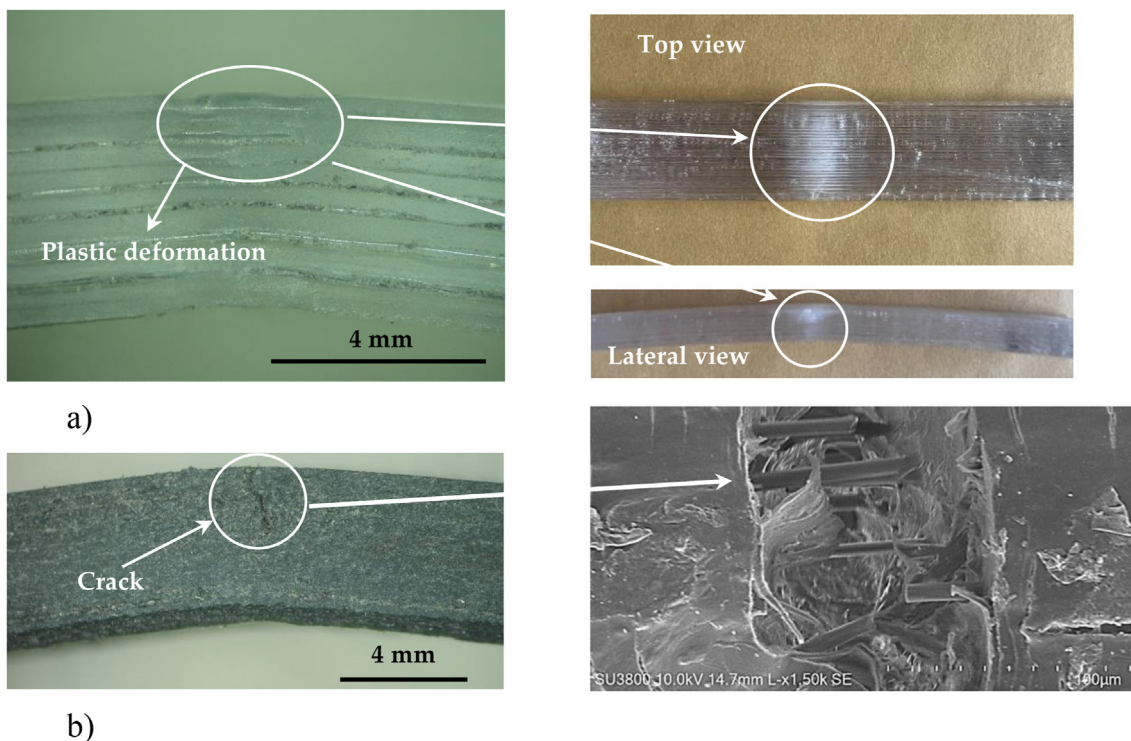


Fig. 10 – Failure modes for: a) Neat PETG; b) PETG + KF composites.

Table 6 – Annealing treatment effect on the bending stress.

Samples Group	PETG		PETG + CF		PETG + KF	
	[MPa]	Variation [%]	[MPa]	Variation [%]	[MPa]	Variation [%]
Control	66.9 ± 1.4	–	79.2 ± 1.0	–	47.7 ± 1.0	–
1	72.6 ± 0.8	8.4	78.3 ± 1.0	–1.2	48.6 ± 1.5	1.8
2	70.7 ± 0.9	5.6	79.8 ± 3.3	0.7	50.1 ± 1.7	4.9
3	68.9 ± 1.2	2.9	81.9 ± 1.8	3.4	51.0 ± 1.8	6.9
4	73.4 ± 1.0	9.7	76.7 ± 1.3	–3.2	49.6 ± 1.0	4.0
5	71.3 ± 1.2	6.6	76.5 ± 3.0	–3.5	52.2 ± 1.3	9.3
6	68.5 ± 3.1	2.4	86.0 ± 2.6	8.5	52.5 ± 3.2	10.1
7	73.7 ± 3.5	10.2	83.7 ± 2.3	5.6	50.5 ± 2.2	5.9
8	71.9 ± 1.0	7.5	97.2 ± 3.3	22.7	52.8 ± 1.6	10.7
9	68.0 ± 1.8	1.6	104.4 ± 3.3	31.8	53.0 ± 1.5	11.1

Table 7 – Annealing treatment effect on the bending modulus.

Samples Group	PETG		PETG + CF		PETG + KF	
	[MPa]	Variation [%]	[MPa]	Variation [%]	[MPa]	Variation [%]
Control	1.7 ± 2.0 × 10 ⁻²	–	3.6 ± 0.2	–	1.5 ± 0.03	–
1	2.0 ± 6.0 × 10 ⁻²	17.6	4.4 ± 0.2	23.0	1.8 ± 0.09	20.2
2	1.9 ± 4.0 × 10 ⁻²	11.8	4.7 ± 0.2	32.0	2.5 ± 0.09	62.6
3	1.9 ± 8.0 × 10 ⁻²	11.8	4.6 ± 0.5	29.0	2.1 ± 0.05	36.3
4	1.8 ± 7.0 × 10 ⁻²	5.9	4.5 ± 0.1	25.3	1.9 ± 0.18	25.7
5	1.8 ± 3.0 × 10 ⁻²	5.9	4.4 ± 0.2	22.6	2.1 ± 0.06	38.9
6	1.8 ± 0.1	5.9	5.1 ± 0.1	43.9	2.1 ± 0.07	34.1
7	2.0 ± 5.0 × 10 ⁻²	17.6	4.9 ± 0.07	39.0	1.8 ± 0.09	20.1
8	1.9 ± 8.0 × 10 ⁻²	11.8	5.4 ± 0.2	51.1	2.2 ± 0.03	46.7
9	1.8 ± 7.0 × 10 ⁻²	5.9	5.8 ± 0.2	61.1	2.2 ± 0.03	46.7

above and the stress levels corresponding to 50% of the maximum bending stress. The average curves were obtained dividing the displacement (D) at any time during the test by the initial displacement (D₀). All curves show an instantaneous displacement, followed by the primary and secondary regimes that characterize typical creep curves. The third regime will be expected to occur only for higher stress values or longer times.

Similar to what was observed for stress relaxation, the neat PETG showed the lowest creep displacement followed by the

PETG + KF and PETG + CF composites with very close values. For example, after 180 min and compared to the neat polymer, the dimensionless creep displacements are 9.5% and 10.2% higher for PETG + KF and PETG + CF composites, respectively. In terms of neat polymer, the creep phenomenon occurs even at room temperature and for stresses below the ultimate strength, which is explained by the molecular motion in backbone polymer arrangement [76–79]. It would be expected that elastic deformation and viscous flow would be delayed with the incorporation of the fibres into the polymer, but this

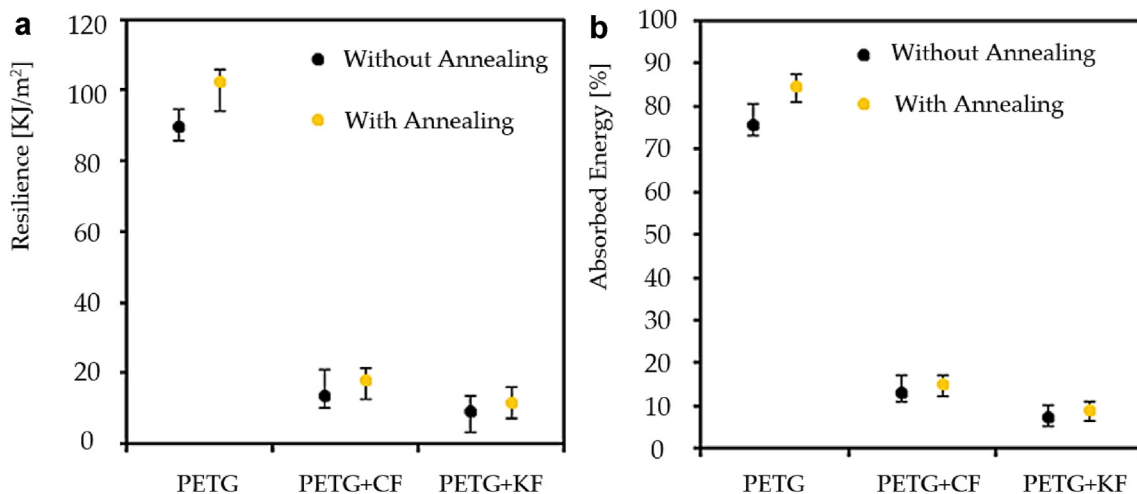


Fig. 11 – Impact response for the different conditions analysed in terms of a) Resilience; b) Absorbed energy.

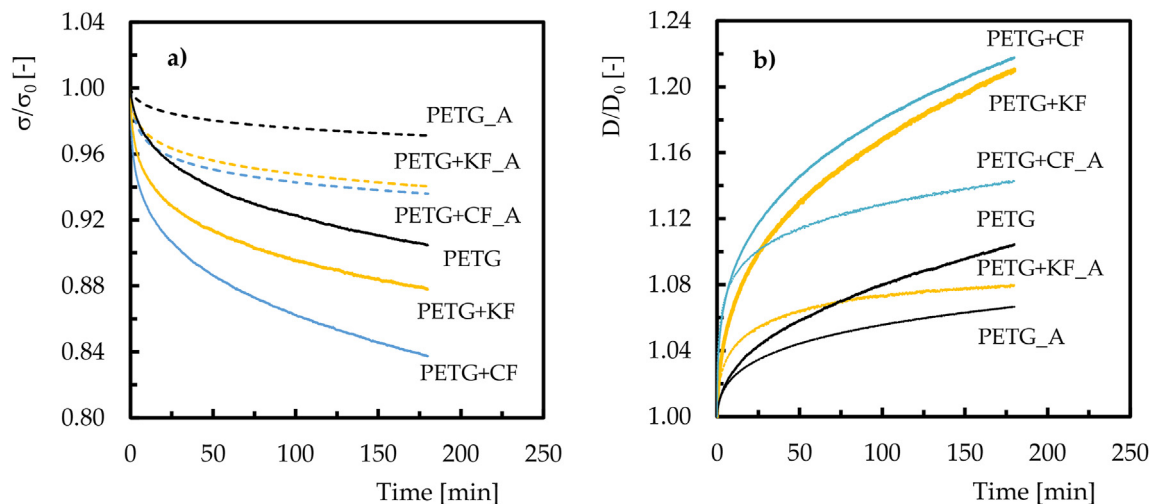


Fig. 12 – a) Stress relaxation curves; b) Creep curves.

phenomenon did not occur for the same reasons explained in detail for stress relaxation. However, after annealing process, all these values decrease. For example, in terms of neat PETG, this treatment decreased the creep displacement after 180 min by around 3.5% compared to untreated specimens, while the creep displacements after annealing are only 1.3% and 7.1% higher for PETG + KF and PETG + CF composites, respectively. In fact, the interlayer adhesion and the fibre/matrix interface prove to be determinants with regard to thermal and mechanical properties [80–82].

4. Conclusions

In this study, the benefits obtained with the annealing process were evaluated through the comparison of the mechanical properties with the geometric changes resulting from this type of treatment. For this purpose, PETG, carbon fibre reinforced PETG (PETG + CF) and Kevlar fibre reinforced PETG (PETG + KF) were used to study the effect of different fibres in this post-process treatment.

It was possible to conclude that, after annealing, the dimensional tolerances were affected. Shrinkage and expansion were observed, regardless of temperature and exposure time, a behaviour that did not change with the presence of fibres. On the other hand, the presence of fibres affects the radius of curvature, but this parameter shows to be very dependent on the type of fibre. In general, lower temperatures and exposure times were found to promote better dimensional stabilization.

In terms of hardness, it generally increased for higher temperatures and longer exposure times. For PETG, the highest increase occurred at 110 °C and 30 min of exposure time, a value 19.2% higher compared to the untreated material. However, for both composites, the improvements were 26.1% and 21.6% for PETG + CF and PETG + KF, respectively, which were obtained at 130 °C and 480 min. Regarding the bending properties, for neat PETG they

increased with temperature and decreased with exposure time, regardless of their value. For composites, they increased with exposure time and temperature. For the maximum bending strength, an increase of 10.2%, 31.8% and 11.1% was observed for neat PETG, PETG + CF and PETG + KF, respectively, compared to the untreated material. In terms of bending modulus, these values are 17.6%, 61.1% and 62.6% respectively.

However, due to design considerations, the geometric effects must be minimized. In this context, optimal annealing conditions were selected, combining the maximization of hardness and bending properties with the minimization of geometric changes. Therefore, based on these premises, materials studied, and values considered, the annealing treatment must be carried out at 90 °C for 30 min for neat PETG and 90 °C and 240 min for composites. Finally, for these values, the annealing treatment increased the impact strength around 8.1%, 3.5% and 16% for neat PETG, PETG + CF and PETG + KF, respectively. Furthermore, this treatment also promotes lower stress relaxation and creep displacement. In terms of stress relaxation, for example, the benefits obtained, in relation to the values obtained with untreated specimens, correspond to values around 71.8%, 64.7% and 54.5% lower for PETG, PETG + CF and PETG + KF, respectively. On the other hand, this treatment decreased the creep displacement by about 3.5% for neat PETG, and the values for PETG + KF and PETG + CF composites are only 1.3% and 7.1% higher (in relation to the neat PETG value), respectively. These improvements are a consequence of the lower content of voids and higher interlayer adhesion obtained with the annealing treatment.

Declaration of competing interest

The authors declare that they have no known competing financial interests or personal relationships that could have appeared to influence the work reported in this paper.

Acknowledgments

This research is sponsored by national funds through FCT—Fundação para a Ciência e a Tecnologia, under the projects UID/EMS/00151/2020 and UIDB/00285/2020.

REFERENCES

- [1] Wu H, Fahy WP, Kim S, Kim H, Zhao N, Pilato L, et al. Recent developments in polymers/polymer nanocomposites for additive manufacturing. *Prog Mater Sci* 2020;111:100638. <https://doi.org/10.1016/j.pmatsci.2020.100638>.
- [2] American Society for Testing and Materials. *ISO/ASTM 52900:2015 – standard terminology for additive manufacturing – general principles – terminology*. West Conshohocken, Pennsylvania: ASTM International; 2015.
- [3] Valvez S, Reis PNB, Susmel L, Berto F. Fused filament fabrication-4D-printed shape memory polymers: a review. *Polymers* 2021;13:701. <https://doi.org/10.3390/polym13050701>.
- [4] Mohamed OA, Masood SH, Bhowmik JL. Optimization of fused deposition modeling process parameters: a review of current research and future prospects. *Adv Manuf* 2015;3:42–53. <https://doi.org/10.1007/s40436-014-0097-7>.
- [5] Valvez S, Santos P, Parente JM, Silva MP, Reis PNB. 3D printed continuous carbon fiber reinforced PLA composites: a short review. *Procedia Struct Integr* 2020;25:394–9. <https://doi.org/10.1016/j.prostr.2020.04.056>.
- [6] Chohan JS, Singh R, Boparai KS, Penna R, Fraternali F. Dimensional accuracy analysis of coupled fused deposition modeling and vapour smoothing operations for biomedical applications. *Compos B Eng* 2017;117:138–49. <https://doi.org/10.1016/j.compositesb.2017.02.045>.
- [7] Love LJ, Kunc V, Rios O, Duty CE, Elliott AM, Post BK, et al. The importance of carbon fiber to polymer additive manufacturing. *J Mater Res* 2014;29:1893–8. <https://doi.org/10.1557/jmr.2014.212>.
- [8] Tekinalp HL, Kunc V, Velez-Garcia GM, Duty CE, Love LJ, Naskar AK, et al. Highly oriented carbon fiber-polymer composites via additive manufacturing. *Compos Sci Technol* 2014;105:144–50. <https://doi.org/10.1016/j.compscitech.2014.10.009>.
- [9] Torrado Perez AR, Roberson DA, Wicker RB. Fracture surface analysis of 3D-printed tensile specimens of novel ABS-based materials. *J Fail Anal Prev* 2014;14:343–53. <https://doi.org/10.1007/s11668-014-9803-9>.
- [10] Ngo TD, Kashani A, Imbalzano G, Nguyen KTQ, Hui D. Additive manufacturing (3D printing): a review of materials, methods, applications and challenges. *Compos B Eng* 2018;143:172–96. <https://doi.org/10.1016/j.compositesb.2018.02.012>.
- [11] Wang P, Pan A, Xia L, Cao Y, Zhang H, Wu W. Effect of process parameters of fused deposition modeling on mechanical properties of poly-ether-ether-ketone and carbon fiber/poly-ether-ether-ketone. *High Perform Polym* 2022;095400832110673. <https://doi.org/10.1177/09540083211067388>.
- [12] Kovan V, Altan G, Topal ES. Effect of layer thickness and print orientation on strength of 3D printed and adhesively bonded single lap joints. *J Mech Sci Technol* 2017;31:2197–201. <https://doi.org/10.1007/s12206-017-0415-7>.
- [13] Anitha R, Arunachalam S, Radhakrishnan P. Critical parameters influencing the quality of prototypes in fused deposition modelling. *J Mater Process Technol* 2001;118:385–8. [https://doi.org/10.1016/S0924-0136\(01\)00980-3](https://doi.org/10.1016/S0924-0136(01)00980-3).
- [14] Nanchariaiah T, Ranga Raju D, Ramachandra Raju V. An experimental investigation on surface quality and dimensional accuracy of FDM components. *Int J Emerg Technol* 2010;1:106–11.
- [15] Gebisa AW, Lemu HG. Investigating effects of fused-deposition modeling (FDM) processing parameters on flexural properties of ULTEM 9085 using designed experiment. *Materials* 2018;11:500. <https://doi.org/10.3390/ma11040500>.
- [16] Ahn S, Montero M, Odell D, Roundy S, Wright PK. Anisotropic material properties of fused deposition modeling ABS. *Rapid Prototyp J* 2002;8:248–57. <https://doi.org/10.1108/13552540210441166>.
- [17] Dawoud M, Taha I, Ebeid SJ. Mechanical behaviour of ABS: an experimental study using FDM and injection moulding techniques. *J Manuf Process* 2016;21:39–45. <https://doi.org/10.1016/j.jmapro.2015.11.002>.
- [18] Torres J, Cotel J, Karl J, Gordon AP. Mechanical property optimization of FDM PLA in shear with multiple objectives. *JOM* 2015;67:1183–93. <https://doi.org/10.1007/s11837-015-1367-y>.
- [19] Bhandari S, Lopez-Anido RA, Gardner DJ. Enhancing the interlayer tensile strength of 3D printed short carbon fiber reinforced PETG and PLA composites via annealing. *Addit Manuf* 2019;30:100922. <https://doi.org/10.1016/j.addma.2019.100922>.
- [20] Diani J, Gall K. Finite strain 3D thermoviscoelastic constitutive model. *Society* 2006:1–10. <https://doi.org/10.1002/pen>.
- [21] Kotsilkova R, Petrova-Doycheva I, Menseidov D, Ivanov E, Paddubskaya A, Kuzhir P. Exploring thermal annealing and graphene-carbon nanotube additives to enhance crystallinity, thermal, electrical and tensile properties of aged poly(lactic) acid-based filament for 3D printing. *Compos Sci Technol* 2019;181:107712. <https://doi.org/10.1016/j.compscitech.2019.107712>.
- [22] Lv S, Gu J, Cao J, Tan H, Zhang Y. Effect of annealing on the thermal properties of poly (lactic acid)/starch blends. *Int J Biol Macromol* 2015;74:297–303. <https://doi.org/10.1016/j.ijbiomac.2014.12.022>.
- [23] Hong J-H, Yu T, Chen Z, Park S-J, Kim Y-H. Improvement of flexural strength and compressive strength by heat treatment of PLA filament for 3D-printing. *Mod Phys Lett B* 2019;33:1940025. <https://doi.org/10.1142/S0217984919400256>.
- [24] Sathish Kumar K, Soundararajan R, Shanthosh G, Saravanakumar P, Ratteesh M, Kumar KS, et al. Augmenting effect of infill density and annealing on mechanical properties of PETG and CFPETG composites fabricated by FDM. *Mater Today Proc* 2021;45:2186–91. <https://doi.org/10.1016/j.matpr.2020.10.078>.
- [25] Magri A El, El Mabrouk K, Vaudreuil S, Touhami ME. Mechanical properties of CF-reinforced PLA parts manufactured by fused deposition modeling. *J Thermoplast Compos Mater* 2021;34:581–95. <https://doi.org/10.1177/0892705719847244>.
- [26] Barkhad MS, Abu-Jdayil B, Mourad AHI, Iqbal MZ. Thermal insulation and mechanical properties of polylactic acid (PLA) at different processing conditions. *Polymers* 2020;12:1–16. <https://doi.org/10.3390/POLYM12092091>.
- [27] D'Amico AA, Debaie A, Peterson AM. Effect of layer thickness on irreversible thermal expansion and interlayer strength in fused deposition modeling. *Rapid Prototyp J* 2017;23:943–53. <https://doi.org/10.1108/RPJ-05-2016-0077>.
- [28] Wang T-M, Xi J-T, Jin Y. A model research for prototype warp deformation in the FDM process. *Int J Adv Manuf Technol* 2007;33:1087–96. <https://doi.org/10.1007/s00170-006-0556-9>.

- [29] Kantaros A, Karalekas D. Fiber Bragg grating based investigation of residual strains in ABS parts fabricated by fused deposition modeling process. *Mater Des* 2013;50:44–50. <https://doi.org/10.1016/j.matdes.2013.02.067>.
- [30] Arjun P, Bidhun VK, Lenin UK, Amritha VP, Pazhamannil RV, Govindan P. Effects of process parameters and annealing on the tensile strength of 3D printed carbon fiber reinforced polylactic acid. *Mater Today Proc* 2022;62:7379–84. <https://doi.org/10.1016/j.matpr.2022.02.142>.
- [31] Valvez S, Silva AP, Reis PNB, Berto F. Annealing effect on mechanical properties of 3D printed composites. *Procedia Struct Integr* 2022;37:738–45. <https://doi.org/10.1016/j.prostr.2022.02.004>.
- [32] Patel P, Rane R, Mrinal M, Ganesan V, Taylor R, Jain A. Characterization of the effect of in-process annealing using a novel print head assembly on the ultimate tensile strength & toughness of Fused Filament Fabrication (FFF) parts. *Virtual Phys Prototyp* 2022;17:989–1005. <https://doi.org/10.1080/17452759.2022.2095288>.
- [33] Valvez S, Silva AP, Reis PNB. Optimization of printing parameters to maximize the mechanical properties of 3D-printed PETG-based parts. *Polymers* 2022;14:2564. <https://doi.org/10.3390/polym14132564>.
- [34] American Society for Testing and Materials. *Astm E 384-22 - standard test method for microindentation hardness of materials*. West Conshohocken, Pennsylvania: ASTM International; 2022.
- [35] American Society for Testing and Materials. *Astm D256 -04 - standard test methods for determining the izod pendulum impact resistance of plastics*. West Conshohocken, Pennsylvania: ASTM International; 2004.
- [36] American Society for Testing and Materials. *Astm d790-17 - standard test methods for flexural properties of unreinforced and reinforced plastics and electrical insulating materials*. West Conshohocken, Pennsylvania: ASTM International; 2017.
- [37] Ferreira JAM, Reis PNB, Costa JDM, Richardson MOW. Fatigue behaviour of Kevlar composites with nanoclay-filled epoxy resin. *J Compos Mater* 2013;47:1885–95. <https://doi.org/10.1177/0021998312452024>.
- [38] American Society for Testing and Materials. *Astm e328-13 - standard test methods for stress relaxation for materials and structures*. West Conshohocken, Pennsylvania: ASTM International; 2013.
- [39] American Society for Testing and Materials. *Astm d2990-09 - standard test methods for tensile, compressive, and flexural creep and creep-rupture of plastics*. West Conshohocken, Pennsylvania: ASTM International; 2009.
- [40] Tantillo AG. *Annealing of fused filament fabricated nylon 6 with elevated isostatic pressure*. Rochester Institute of Technology; 2019.
- [41] Zhang Y, Moon SK. The effect of annealing on additive manufactured ULTEM™ 9085 mechanical properties. *Materials* 2021;14:2907. <https://doi.org/10.3390/ma14112907>.
- [42] Butt J, Bhaskar R. Investigating the effects of annealing on the mechanical properties of FFF-printed thermoplastics. *Journal of Manufacturing and Materials Processing* 2020;4:1–20. <https://doi.org/10.3390/jmmp4020038>.
- [43] Tirado-Garcia I, Garcia-Gonzalez D, Garzon-Hernandez S, Rusinek A, Robles G, Martinez-Tarifa JM, et al. Conductive 3D printed PLA composites: on the interplay of mechanical, electrical and thermal behaviours. *Compos Struct* 2021;265:113744. <https://doi.org/10.1016/j.compstruct.2021.113744>.
- [44] Yang L, Li S, Zhou X, Liu J, Li Y, Yang M, et al. Effects of carbon nanotube on the thermal, mechanical, and electrical properties of PLA/CNT printed parts in the FDM process. *Synth Met* 2019;253:122–30. <https://doi.org/10.1016/j.synthmet.2019.05.008>.
- [45] Hu B, Duan X, Xing Z, Xu Z, Du C, Zhou H, et al. Improved design of fused deposition modeling equipment for 3D printing of high-performance PEEK parts. *Mech Mater* 2019;137:103139. <https://doi.org/10.1016/j.mechmat.2019.103139>.
- [46] Peng A. Research on the interlayer stress and warpage deformation in FDM. *Adv Mater Res* 2012;538–541:1564–7. <https://doi.org/10.4028/www.scientific.net/AMR.538-541.1564>.
- [47] Ahmadifar M, Benfriha K, Shirinbayan M, Tcharkhtchi A. Additive manufacturing of polymer-based composites using fused filament fabrication (FFF): a review. *Appl Compos Mater* 2021;28:1335–80. <https://doi.org/10.1007/s10443-021-09933-8>.
- [48] Goh GD, Yap YL, Tan HKJ, Sing SL, Goh GL, Yeong WY. Process–structure–properties in polymer additive manufacturing via material extrusion: a review. *Crit Rev Solid State Mater Sci* 2020;45:113–33. <https://doi.org/10.1080/10408436.2018.1549977>.
- [49] Brenken B, Barocio E, Favaloro A, Kunc V, Pipes RB. Fused filament fabrication of fiber-reinforced polymers: a review. *Addit Manuf* 2018;21:1–16. <https://doi.org/10.1016/j.addma.2018.01.002>.
- [50] Ma S, Yang H, Zhao S, He P, Zhang Z, Duan X, et al. 3D-printing of architected short carbon fiber-geopolymer composite. *Compos B Eng* 2021;226:109348. <https://doi.org/10.1016/j.compositesb.2021.109348>.
- [51] Cisneros-López EO, Pal AK, Rodríguez AU, Wu F, Misra M, Mielewski DF, et al. Recycled poly(lactic acid)-based 3D printed sustainable biocomposites: a comparative study with injection molding. *Materials Today Sustainability* 2020;7–8:100027. <https://doi.org/10.1016/j.mtsust.2019.100027>.
- [52] de Gennes PG. Reptation of a polymer chain in the presence of fixed obstacles. *J Chem Phys* 1971;55:572–9. <https://doi.org/10.1063/1.1675789>.
- [53] Kim YH, Wool RP. A theory of healing at a polymer-polymer interface. *Macromolecules* 1983;16:1115–20. <https://doi.org/10.1021/ma00241a013>.
- [54] Sun Q, Rizvi GM, Bellehumeur CT, Gu P. Effect of processing conditions on the bonding quality of FDM polymer filaments. *Rapid Prototyp J* 2008;14:72–80. <https://doi.org/10.1108/13552540810862028>.
- [55] Prager S, Tirrell M. The healing process at polymer–polymer interfaces. *J Chem Phys* 1981;75:5194–8. <https://doi.org/10.1063/1.441871>.
- [56] Perego G, Cella GD, Bastioli C. Effect of molecular weight and crystallinity on poly(lactic acid) mechanical properties. *J Appl Polym Sci* 1996;59:37–43. [https://doi.org/10.1002/\(SICI\)1097-4628\(19960103\)59:1<37::AID-APP6>3.0.CO;2-N](https://doi.org/10.1002/(SICI)1097-4628(19960103)59:1<37::AID-APP6>3.0.CO;2-N).
- [57] Geng P, Zhao J, Wu W, Wang Y, Wang B, Wang S, et al. Effect of thermal processing and heat treatment condition on 3D printing PPS properties. *Polymers* 2018;10:875. <https://doi.org/10.3390/polym10080875>.
- [58] El Magri A, El Mabrouk K, Vaudreuil S, Chibane H, Touhami ME. Optimization of printing parameters for improvement of mechanical and thermal performances of 3D printed poly(ether ether ketone) parts. *J Appl Polym Sci* 2020;137:1–14. <https://doi.org/10.1002/app.49087>.
- [59] Yang C, Tian X, Li D, Cao Y, Zhao F, Shi C. Influence of thermal processing conditions in 3D printing on the crystallinity and mechanical properties of PEEK material. *J Mater Process Technol* 2017;248:1–7. <https://doi.org/10.1016/j.jmatprotec.2017.04.027>.
- [60] Ferreira I, Melo C, Neto R, Machado M, Alves JL, Mould S. Study of the annealing influence on the mechanical

- performance of PA12 and PA12 fibre reinforced FFF printed specimens. *Rapid Prototyp J* 2020;26:1761–70. <https://doi.org/10.1108/RPJ-10-2019-0278>.
- [61] Pazhamannil RV, Krishnan CN, P G, Edacherian A. Investigations into the effect of thermal annealing on fused filament fabrication process. *Advances in Materials and Processing Technologies* 2021;1–14. <https://doi.org/10.1080/2374068X.2021.1946753>.
- [62] Ivey M, Melenka GW, Carey JP, Ayranci C. Characterizing short-fiber-reinforced composites produced using additive manufacturing. *Adv Manuf Polym Compos Sci* 2017;3:81–91. <https://doi.org/10.1080/20550340.2017.1341125>.
- [63] Wickramasinghe S, Do T, Tran P. FDM-based 3D printing of polymer and associated composite: a review on mechanical properties, defects and treatments. *Polymers* 2020;12:1529. <https://doi.org/10.3390/polym12071529>.
- [64] Singh S, Singh M, Prakash C, Gupta MK, Mia M, Singh R. Optimization and reliability analysis to improve surface quality and mechanical characteristics of heat-treated fused filament fabricated parts. *Int J Adv Manuf Technol* 2019;102:1521–36. <https://doi.org/10.1007/s00170-018-03276-8>.
- [65] Monjon A, Santos P, Valvez S, Reis PNB. Hybridization effects on bending and interlaminar shear strength of composite laminates. *Materials* 2022;15:1302. <https://doi.org/10.3390/ma15041302>.
- [66] Reis PNB, Soares JRL, Pereira AM, Ferreira JAM. Effect of adherends and environment on static and transverse impact response of adhesive lap joints. *Theor Appl Fract Mech* 2015;80:79–86. <https://doi.org/10.1016/j.tafmec.2015.07.004>.
- [67] Kumar KR, Mohanavel V, Kiran K. Mechanical properties and characterization of polylactic acid/carbon fiber composite fabricated by fused deposition modeling. *J Mater Eng Perform* 2022. <https://doi.org/10.1007/s11665-021-06566-7>.
- [68] Kamaal M, Anas M, Rastogi H, Bhardwaj N, Rahaman A. Effect of FDM process parameters on mechanical properties of 3D-printed carbon fibre–PLA composite. *Progress in Additive Manufacturing* 2021;6:63–9. <https://doi.org/10.1007/s40964-020-00145-3>.
- [69] Reis PNB, Silva MP, Santos P, Parente JM, Valvez S, Bezazi A. Mechanical performance of an optimized cork agglomerate core-glass fibre sandwich panel. *Compos Struct* 2020;245:112375. <https://doi.org/10.1016/j.compstruct.2020.112375>.
- [70] Varghese S, Kuriakose B, Thomas S. Stress relaxation in short sisal-fiber-reinforced natural rubber composites. *J Appl Polym Sci* 1994;53:1051–60. <https://doi.org/10.1002/app.1994.070530807>.
- [71] George J, Sreekala MS, Thomas S, Bhagawan SS, Neelakantan NR. Stress relaxation behavior of short pineapple fiber reinforced polyethylene composites. *J Reinforc Plast Compos* 1998;17:651–72. <https://doi.org/10.1177/073168449801700704>.
- [72] Sreekala MS, Kumaran MG, Joseph R, Thomas S. Stress-relaxation behaviour in composites based on short oil-palm fibres and phenol formaldehyde resin. *Compos Sci Technol* 2001;61:1175–88. [https://doi.org/10.1016/S0266-3538\(00\)00214-1](https://doi.org/10.1016/S0266-3538(00)00214-1).
- [73] Valvez S, Silva AP, Reis PNB. Compressive behaviour of 3D-printed PETG composites. *Aerospace* 2022;9:124. <https://doi.org/10.3390/aerospace9030124>.
- [74] Obaid N, Kortschot M, Sain M. Understanding the stress relaxation behavior of polymers reinforced with short elastic fibers. *Materials* 2017;10:472. <https://doi.org/10.3390/ma10050472>.
- [75] Al Rashid A, Koç M. Creep and recovery behavior of continuous fiber-reinforced 3DP composites. *Polymers* 2021;13:1644. <https://doi.org/10.3390/polym13101644>.
- [76] Wang W-H, Huang H-B, Du H-H, Wang H. Effects of fiber size on short-term creep behavior of wood fiber/HDPE composites. *Polym Eng Sci* 2015;55:693–700. <https://doi.org/10.1002/pen.23935>.
- [77] Park B-D, Balatinez JJ. Short term flexural creep behavior of wood-fiber/polypropylene composites. *Polym Compos* 1998;19:377–82. <https://doi.org/10.1002/pc.10111>.
- [78] Houshyar S, Shanks RA, Hodzic A. Tensile creep behaviour of polypropylene fibre reinforced polypropylene composites. *Polym Test* 2005;24:257–64. <https://doi.org/10.1016/j.polymertesting.2004.07.003>.
- [79] Bouafif H, Koubaa A, Perré P, Cloutier A. Creep behaviour of HDPE/wood particle composites. *Int J Microstruct Mater Prop* 2013;8:225–38. <https://doi.org/10.1504/IJMMP.2013.055385>.
- [80] Yao B, Imani F, Sakpal AS, Reutzel EW, Yang H. Multifractal analysis of image profiles for the characterization and detection of defects in additive manufacturing. *J Manuf Sci Eng* 2018;140:1–21. <https://doi.org/10.1115/1.4037891>.
- [81] Braga RA, Magalhaes PAA. Analysis of the mechanical and thermal properties of jute and glass fiber as reinforcement epoxy hybrid composites. *Mater Sci Eng C* 2015;56:269–73. <https://doi.org/10.1016/j.msec.2015.06.031>.
- [82] Blok LG, Longana ML, Yu H, Woods BKS. An investigation into 3D printing of fibre reinforced thermoplastic composites. *Addit Manuf* 2018;22:176–86. <https://doi.org/10.1016/j.addma.2018.04.039>.